Measuring Organic Molecular Emission in Disks with Low Resolution Spitzer Spectroscopy

Johanna K. Teske

Steward Observatory, University of Arizona, 933 N. Cherry Avenue, Tucson, AZ 85721, USA jteske@as.arizona.edu

Joan R. Najita

National Optical Astronomy Observatory, 950 N. Cherry Avenue, Tucson, AZ 85716, USA
najita@noao.edu

John S. Carr

Naval Research Laboratory, Code 7211, Washington, DC 20375, USA

carr@nrl.navy.mil

Ilaria Pascucci

Space Telescope Science Institute, 3700 San Martin Drive, Baltimore, MD 21218, USA pascucci@stsci.edu

Daniel Apai

Space Telescope Science Institute, 3700 San Martin Drive, Baltimore, MD 21218, USA apai@stsci.edu

and

Thomas Henning

Max-Planck-Institut für Astronomie, Königstuhl 17, 69117 Heidelberg, Germany

henning@mpia.de

ABSTRACT

We explore the extent to which *Spitzer* IRS spectra taken at low spectral resolution can be used in quantitative studies of organic molecular emission from disks surrounding low mass young stars. We use *Spitzer* IRS spectra taken in both the high and low resolution modules for the same sources to investigate whether it is possible to define

line indices that can measure trends in the strength of the molecular features in low resolution data. We find that trends in HCN emission strength seen in the high resolution data can be recovered in low resolution data. In examining the factors that influence the HCN emission strength, we find that the low resolution HCN flux is modestly correlated with stellar accretion rate and X-ray luminosity. Correlations of this kind are perhaps expected based on recent observational and theoretical studies of inner disk atmospheres. Our results demonstrate the potential of using the large number of low resolution disk spectra that reside in the *Spitzer* archive to study the factors that influence the strength of molecular emission from disks. Such studies would complement results for the much smaller number of circumstellar disks that have been observed at high resolution with IRS.

Subject headings: infrared: stars — (stars:) circumstellar matter — stars: pre-main sequence — stars: formation — planetary systems: protoplanetary disks

1. Introduction

Circumstellar disks composed of gas and dust are ubiquitous around forming stars and are the birthplace of planets. Since habitable planets are expected to form in warm inner disks (< 3–4 AU for sun-like stars), studying this region is especially relevant to understanding the origin and evolution of habitable planetary systems and their diverse properties. Interest in the origin of stars and planets has lead to numerous studies of the gaseous components of disks at large (> 20 AU) radial distances (e.g., Dutrey et al. 1996, 1998, 2007; Kastner et al. 1997; Guilloteau & Dutrey 1998; Thi et al. 2004; Semenov et al. 2005; Qi et al. 2008) as well as warmer, solid components within ~ 10 AU of the star (e.g., Natta et al. 2007; Henning & Meeus 2009; Apai & Lauretta 2010).

Observations of the warm gas within the inner disk are also necessary to fully understand the structure and dynamics affecting disk evolution and planet formation (see Carr 2005; Najita et al. 2007a; Millan-Gabet et al. 2007; Carmona 2010 for recent reviews). When such gas is viewed in emission from disks around T Tauri stars (TTS), which are optically thick in the continuum at small disk radii ($< 10\,\mathrm{AU}$), the emission likely originates in a temperature inversion region at the disk surface. The very inner regions of the gaseous disk ($< 0.3\,\mathrm{AU}$) have been studied previously using molecular transitions such as CO overtone emission (e.g., Carr et al. 1993; Chandler et al. 1993; Najita et al. 1996, 2000, 2009; Blum et al. 2004; Thi et al. 2005; Thi & Bik 2005; Berthoud et al. 2007) and ro-vibrational $\mathrm{H_2O}$ emission (e.g., Carr et al. 2004; Najita et al. 2000, 2009; Thi & Bik 2005). Observations of CO fundamental emission (e.g., Carr et al. 2001; Najita et al. 2003, 2008; Blake & Boogert 2004; Brittain et al. 2007; Salyk et al. 2007, 2009; Pontoppidan et al. 2008) and UV transitions of $\mathrm{H_2}$ (e.g., Valenti et al. 2000; Ardila & Basri 2000; Herczeg et al. 2002, 2006; Bergin et al. 2004) have been used to probe larger disk radii (out to $\sim 1-2\,\mathrm{AU}$).

More recently, observations of T Tauri disks made with the high resolution $(R \sim 700)$ modules

of the Infrared Spectrograph (IRS) on board the Spitzer Space Telescope (Houck et al. 2004) have revealed that simple organic molecules (HCN, C_2H_2 , CO_2) and water (Lahuis et al. 2006; Carr & Najita 2008; Salyk et al. 2008) are present in the warm inner disk region ($\lesssim 5 \,\mathrm{AU}$). IRS observations indicate that mid-infrared molecular emission is common among TTS (Pontoppidan et al. 2010; Carr & Najita 2011; see also Pascucci et al. 2009 in the context of low resolution IRS data) and can be used to probe the thermal and chemical structure of the inner gaseous disk (see Figure 1).

With the cryogen of the *Spitzer Space Telescope* depleted, it is no longer possible to obtain more sensitive, mid-infrared spectroscopy of protoplanetary disks, making the *Spitzer* archive the primary source of new information on warm disk chemistry. However, with most of the data in the archive taken in low-resolution mode, the question emerges: How much information regarding molecular emission features can be extracted from the low-resolution observations? Pascucci et al. (2009) previously explored this question, showing that molecular emission could be detected in low resolution IRS spectra of dozens TTS and lower-mass stars and brown dwarfs. They found that HCN emission at $14 \,\mu m$ was almost always brighter than C_2H_2 emission at $13.7 \,\mu m$ among T Tauri stars, while only C_2H_2 and no HCN was detected for lower mass stars and brown dwarfs. This led them to propose that there are differences in the relative abundance of molecular species as a function of stellar mass.

Here we build upon the work of Pascucci et al. (2009) by investigating the extent to which we can extract quantitative information from low resolution *Spitzer* IRS spectra of inner T Tauri disks. To do this, we compare the molecular emission strength in a sample of high resolution IRS spectra of T Tauri stars with similar measurements of the same sources made in the low resolution mode of IRS. If quantitative trends in the strength of molecular emission features can be recovered from low resolution spectra, the archival *Spitzer* IRS data could be used to study the strength of molecular features in disks. Since, as we discuss below, a variety of physical and chemical processes can potentially affect the molecular emission strength, spectra of large samples of sources, such as those available in the *Spitzer* archive, are a valuable asset for demographic studies that seek to identify the dominant processes influencing the molecular emission from disks. In §2 we describe the data sets used in this paper. In §3 we present our method of analysis and our results. The latter are explored further in §4.

2. Data Sets

For our comparison of high and low resolution data, we examined a small set of *Spitzer IRS* spectra of T Tauri stars in the Taurus-Auriga star-forming region. The higher resolution data were taken with IRS in the short-high mode (SH, $10-19\,\mu\text{m}$, $R\sim700$), and the lower resolution data were taken in the short-low mode (SL, $5.2-14\,\mu\text{m}$, $R\sim100$). Our SH data set was selected from classical T Tauri stars that were observed as part of the Cycle 2 GO Program 20363 (Carr & Najita 2008, 2011). From 11 sources in that program, we selected a sample of "normal" T Tauri stars, i.e, sources with stellar accretion rates $\lesssim 10^{-7}~\text{M}_{\odot}\text{yr}^{-1}$, to avoid the influence of highly energetic

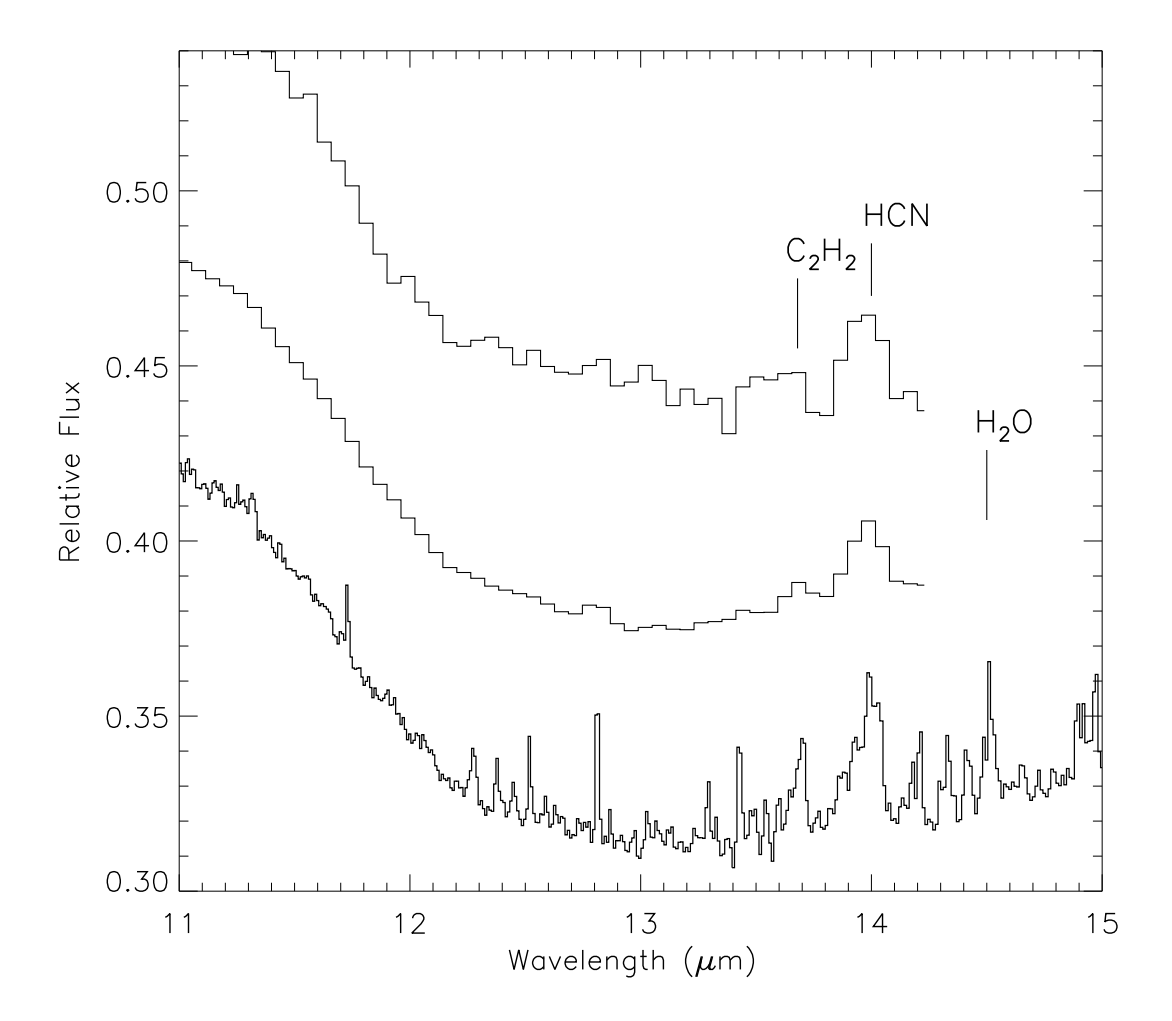


Fig. 1.— The $11-15\,\mu\mathrm{m}$ spectrum of AA Tau as observed in the SH ($R\sim700$, bottom) and SL ($R\sim100$, top) modes. The middle spectrum is the SH spectrum smoothed to the resolution of the SL data and rebinned to the pixel sampling of the SL data. Several prominent molecular features are marked with vertical lines. The high resolution data reveal a rich emission spectrum that is common among TTS. We show that trends in HCN emission strength in high resolution spectra can be recovered from lower resolution data.

accretion processes (e.g., jets) on the spectrum. We also excluded close binary stars (the closest companion separation in our sample is 0.88") since tidal interactions between the disk and binary can disrupt or truncate the inner disk region ($< 5\,\mathrm{AU}$). The resulting 8 sources display mid-infrared colors that are typical of "normal" TTS. That is, they have colors that are unlike those of transition objects. Specifically, as described in Furlan et al. (2006), our sample has n_{6-13} between -1.0 and -0.01, and n_{13-25} between -0.40 and 0.17, where n_{6-13} and n_{13-25} are the $6-13\,\mu\mathrm{m}$ and $13-25\,\mu\mathrm{m}$ colors, respectively.

To compare with the 8 SH spectra, we examined SL spectra of the same objects, originally observed as part of the *Spitzer* GO Program 2 (P.I. Houck). We used the reduced SL spectra from Pascucci et al. (2009). The observations were originally published as part of a larger data set by Furlan et al. (2006) using an alternative reduction procedure that they detail. Since the molecular emission features were not the focus of the latter study, those spectra were not as reliable in the $13-15\,\mu\mathrm{m}$ region.

In order to determine the processes that might influence the strength of any observed molecular emission, we also examined SL spectra of an additional 10 sources from the Pascucci et al. (2009) sample that have stellar properties similar to those of the SH sample: accretion rates within an order of magnitude of the typical T Tauri rate $10^{-8}~\rm M_{\odot} yr^{-1}$ (Hartmann et al. 1998), an absence of close companions, and normal mid-infrared colors. While the full sample of 18 SL sources is relatively uniform in infrared spectral shape, binarity, and spectral type, it exhibits more variety in stellar accretion rate and X-ray luminosity (see Table 1). The stellar accretion rates in Table 1 are from Hartmann et al. (1998) and Najita et al. (2007b). Najita et al. adopted stellar accretion rates from several literature sources and placed them on the same scale as Hartmann et al., providing a set of comparable, consistent values. The X-ray luminosities are from the recent reanalysis of Güdel et al. (2010) of XMM-Newton and Chandra observations of a large number of T Tauri stars. The X-ray luminosities are for the 0.3–10 keV range and have been corrected for line-of-sight absorption (Güdel et al. 2010). We also assume a distance of 140 pc. The properties of our full sample are described in Table 1.

Table 1. Our T Tauri Sample

Object	Spectral Type ^{a}	$\log(\dot{M}_*/M_{\odot}yr^{-1})^c$	$\log(L_{\rm X}/{\rm erg~s^{-1}})^e$	IRS Mode	
AA Tau	K7	-8.48	30.01	SH, SL	
BP Tau	K7	-7.54	30.16	SH, SL	
CW Tau	K3	-7.61		SL	
CX Tau	M2.5	-8.97		SL	
CY Tau	M1	-8.12		SL	
DK Tau	K7	-7.42	29.93	SH, SL	
DN Tau	M0	-8.46	30.03	SL	
DO Tau	M0	-6.85	29.37	SH, SL	
DP Tau	M0.5	-7.88	28.99	SL	
DS Tau	K5	-7.89		SL	
FZ Tau	$\mathrm{M0}^{b}$	-7.32		SL	
GI Tau	K6	-8.02^{d}	29.82	SH, SL	
GK Tau	K7	-8.19	30.09	SH, SL	
HN Tau	K5	-8.89^{d}	29.50	SL	
IP Tau	M0	-9.10		SL	
IQ Tau	M0.5	-7.55	29.50	SL	
RW Aur	K3	-7.12	30.21	SH, SL	
UY Aur	K7	-7.18	29.60	SH, SL	

References. — (a) Kenyon & Hartmann (1995), unless otherwise noted; (b) Hartigan et al. (1994); (c) Najita et al. (2007b), unless otherwise noted; (d) Hartmann et al. (1998); (e) Güdel et al. (2010), corrected for line-of-sight absorption and assuming a distance of 140 pc

3. Analysis and Results

3.1. SH vs. SL Measurements

As described in §1, Pascucci et al. (2009) previously showed that the $14 \,\mu\mathrm{m}$ HCN feature is almost always brighter than the $13.7 \,\mu\mathrm{m}$ C₂H₂ feature in T Tauri spectra, making it typically the most apparent feature at low spectral resolution. Thus, while we investigated the possibility of detecting the emission from several molecules (HCN, C₂H₂, H₂O) in the SL data, we chose to focus in this paper on HCN due to its greater detectability in our sample.

To estimate the strength of the HCN feature, we defined a feature index based on the structure seen in existing SH spectra and synthetic disk emission models (e.g., Carr & Najita 2008) to avoid contamination from neighboring molecular features. We selected the wavelengths $13.885 \,\mu\mathrm{m}$ and $14.062 \,\mu\mathrm{m}$ to define the boundaries of the HCN feature. To estimate the underlying continuum, we found the average flux density in two neighboring regions, $13.776-13.808 \,\mu\mathrm{m}$ and $14.090-14.126 \,\mu\mathrm{m}$, assigned these values to the midpoint of each region, and performed a linear fit to these two midpoints. We subtracted the continuum estimate from the spectrum and summed the resulting spectrum within the wavelength boundaries of the feature to obtain the feature flux. The equivalent width of the feature was calculated in a corresponding way. These values are reported in Tables 2 & 3. In the SH spectra, the continuum regions each span three pixels and the HCN feature spans fifteen pixels, while in the SL spectra the continuum regions each span less than one pixel and the HCN feature spans three pixels (see Figure 2).

The errors on the SH spectra are described in Carr & Najita (2011). They are derived from the average RMS pixel variation around $14\,\mu\mathrm{m}$. To estimate the errors on the SL spectra, we performed a linear fit to the continuum over ~ 15 pixels between $13\,\mu\mathrm{m}$ and $14.2\,\mu\mathrm{m}$, excluding the regions around HCN (13.885 $\mu\mathrm{m}-14.062\,\mu\mathrm{m}$) and $\mathrm{C_2H_2}$ (13.609 $\mu\mathrm{m}-13.736\,\mu\mathrm{m}$), and used the standard deviation of the difference between the observed spectrum and the fit as a measure of the pixel-to-pixel noise. We quote this measurement as our 1σ errors in Table 2. These errors are generally smaller than those reported by Pascucci et al. (2009), who adopted an error for each pixel based on the difference in flux observed in a small number (2) of nod positions.

In Table 2 we show the SL fluxes, equivalent widths, and errors determined using the feature and continuum regions defined above. Objects for which we have SH data are listed in Table 3

¹ This latter error estimate can be affected by flux differences in the two beam positions if the object is not equally centered in the slit in each beam position. Some of the spectra appeared to suffer from this effect as the estimated errors were often larger than the pixel-to-pixel differences in the final spectrum (e.g., CW Tau, CY Tau, DN Tau, GI Tau, GK Tau, IP Tau). While our errors are generally smaller than the Pascucci et al. (2009) errors, our adopted errors may still overestimate the true error. That is because our approach assumes that the true spectrum is featureless in the region used to estimate the pixel-to-pixel variation (i.e., in the regions around the HCN and C_2H_2 features), whereas the spectra may in fact have a rich spectrum of weaker emission features (Fig. 1). We return to this issue below.

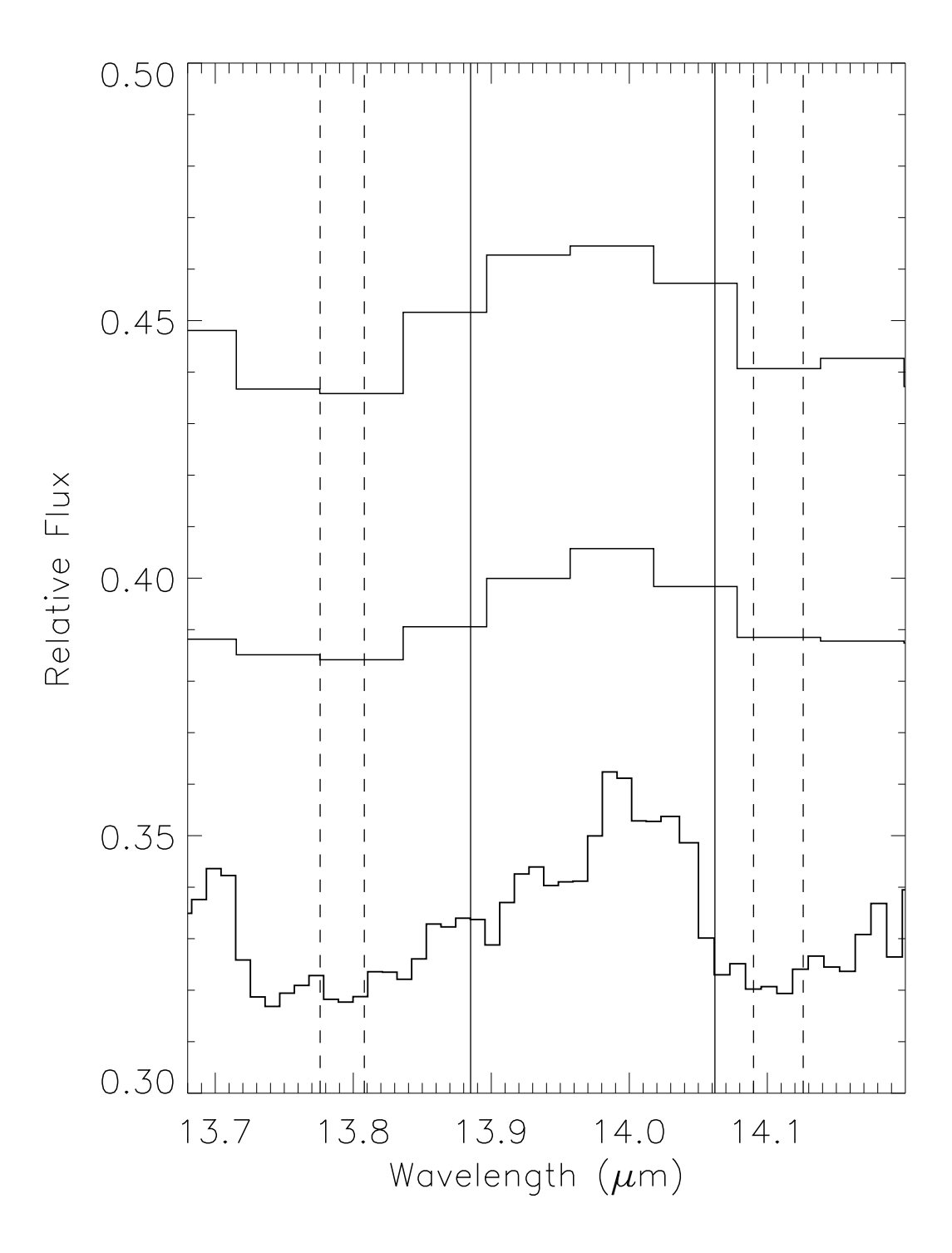


Fig. 2.— Spectrum of AA Tau comparing SH (bottom), smoothed and resampled (middle), and SL (top) data in the region around the $14\,\mu\mathrm{m}$ HCN feature. The dotted vertical lines indicate the left and right continuum regions, and the vertical lines define the HCN feature, as listed in §3.

along with their flux and equivalent width measurements.

To understand any difference between these two data sets, we first smoothed the SH spectra to the approximate resolution of the SL spectra ($R \sim 100$) by convolving with a Gaussian profile and rebinned to match the SL pixel sampling. As these two data sets are "contemporaneous" (they are the same data), comparing them avoids any complications arising from time variability in the mid-infrared emission spectrum. We find that the fluxes and equivalent widths of the smoothed/resampled data are on average $\sim 50\%$ of those measured for the SH data (Fig. 3a). The lower values for the smoothed/resampled data are the result of the neighboring line emission from water and other features (Fig. 1; Carr & Najita 2008, 2011; Pontoppidan et al. 2010), which blends into a pseudo-continuum at lower spectral resolution, diluting the HCN flux and equivalent width. Because the neighboring line emission can vary from source to source in both shape and strength relative to HCN (stronger or weaker neighboring emission lines), there is dispersion about the $\sim 50\%$ average value.

We would expect that the effect of the lower spectral resolution would lead to a similar difference between the SH measurements and those made on the real SL data. An additional factor in comparing the SH data with the (non-contemporaneous) SL data is the possibility of time variability in the HCN and/or non-HCN line emission spectrum, which would increase the dispersion beyond that arising from the lower resolution alone. This is indeed the case. The comparison of the SL equivalent widths shows more dispersion than the smoothed/resampled data when compared against the SH data (Fig. 3b). Figure 3c shows that the lower average equivalent width of the smoothed/resampled data does indeed capture the trend of the reduction in the SL equivalent width. Similar results are found for the HCN fluxes of the SH, smoothed/resampled, and SL data sets.

The HCN equivalent width and flux measurements from the SH and SL data are well correlated (Figure 3 and Table 4). To assess the significance of the apparent trends, we use two correlation coefficients, Kendall's rank correlation coefficient, $\tau_{Kendall}$, and Pearson's linear correlation coefficient, r. The former, $\tau_{Kendall}$, is a non-parametric statistic that measures the degree of correlation between two variables; values close to unity signify a tighter correlation, while values close to 0 signify no correlation. Our calculated $\tau_{Kendall}$ -values are all ≥ 0.59 . The two-sided P values that correspond to $\tau_{Kendall}$, P_{τ} , represent the confidence levels of the coefficient – a smaller P value indicates a lower probability of a false conclusion. Pearson's r-value measures how closely two parameters fit a linear relationship (assuming the parameter distributions are normal). The closer |r| is to unity, the more linear the relationship. Our calculated r-values are all ≥ 0.80 , signifying a near-linear correlation. We also calculate p_{rand} (as a %), the probability that our measurements are randomly distributed (and thus uncorrelated). The calculated p_{rand} values, $\sim 1.8\%$ and 7.0% for the equivalent width and flux relations, respectively, indicate that it is highly unlikely that our measurements are randomly distributed. These statistics for the above trends are shown in Table 4. As we suspect and the figures indicate, the trends we find are statistically significant.

Table 2. HCN Short-Low Measurements

Object	SL HCN Flux (mJy-μm)	SL HCN EW $(10^{-3} \mu m)$
AA Tau	4.00 ± 0.66	10.6 ± 1.77
BP Tau	2.43 ± 0.34	5.77 ± 0.81
CW Tau	3.17 ± 0.77	4.15 ± 1.02
CX Tau	-0.178 ± 0.53	-1.16 ± 3.35
CY Tau	-0.170 ± 0.54	-1.47 ± 4.60
DK Tau	1.75 ± 0.70	1.96 ± 0.78
DN Tau	2.20 ± 0.39	7.04 ± 1.28
DO Tau	1.87 ± 1.27	1.19 ± 0.81
DP Tau	0.608 ± 0.66	1.03 ± 1.11
DS Tau	2.33 ± 0.23	9.65 ± 0.99
FZ Tau	4.37 ± 1.38	4.93 ± 1.58
GI Tau	2.99 ± 0.62	4.09 ± 0.85
GK Tau	-1.13 ± 0.77	-1.37 ± 0.93
HN Tau	0.783 ± 0.59	0.992 ± 0.75
IP Tau	-0.964 ± 0.69	-5.26 ± 3.75
IQ Tau	2.02 ± 0.62	6.07 ± 1.90
RW Aur	5.51 ± 1.34	4.32 ± 1.06
UY Aur	2.62 ± 1.30	0.871 ± 0.43

Table 3. HCN Short-High and Smoothed & Resampled Measurements

Object	SH HCN Flux (mJy- μ m)	SH HCN EW $(10^{-3} \mu \text{m})$	SM+RS HCN Flux (mJy-μm)	SM+RS HCN EW $(10^{-3} \mu \text{m})$
AA Tau	4.43 ± 0.08	13.9 ± 0.25	2.52 ± 0.06	7.72 ± 0.18
BP Tau	4.31 ± 0.08	11.6 ± 0.21	2.35 ± 0.06	6.21 ± 0.15
DK Tau	5.01 ± 0.15	6.59 ± 0.19	2.20 ± 0.10	2.86 ± 0.13
DO Tau	1.32 ± 0.25	0.653 ± 0.12	-0.676 ± 0.12	-0.333 ± 0.09
GI Tau	4.69 ± 0.12	6.18 ± 0.15	2.47 ± 0.08	3.22 ± 0.11
GK Tau	0.850 ± 0.15	1.07 ± 0.15	0.104 ± 0.09	0.130 ± 0.11
RW Aur	9.36 ± 0.25	6.32 ± 0.17	3.97 ± 0.18	2.64 ± 0.12
UY Aur	5.95 ± 0.34	2.24 ± 0.12	1.56 ± 0.24	0.58 ± 0.09

Table 4. Correlation Between SH and SL HCN Emission

Parameters		$r^{ m b}$	$ au_{Kendall}{}^{\mathrm{c}}$	P_{τ}^{d}	p_{rand} (%) ^e
SH vs. SL EW	8	0.904	0.714	0.019	1.77
SH vs. SL Flux	8	0.797	0.590	0.108	7.01
Smoothed vs. SL EW	8	0.908	0.714	0.019	1.64

^a The number of objects used for calculation of the statistic.

Table 5. Correlations Between Stellar Parameters & SL HCN Emission

Parameters	Points Rejected	na	$r^{ m b}$	$ au_{Kendall}{}^{\mathrm{c}}$	P_{τ}^{d}	p_{rand} (%) $^{\mathrm{e}}$	χ^2	q
$\log(\dot{M}_*/M_{\odot}yr^{-1})$ vs. SL Flux – initial fit	none	18	0.534	0.386	0.028	8.42	1.17	0.280
$\log(\dot{M}_*/M_{\odot} yr^{-1})$ vs. SL Flux – final fit	2	16	0.655	0.567	0.178	2.87	0.753	0.721
$\log(L_{\rm X}/{\rm erg~s^{-1}})$ vs. SL Flux – initial fit	none	12	0.403	0.382	0.099	34.19	1.37	0.186
$\log(L_{\rm X}/{\rm erg~s^{-1}})$ vs. SL Flux – final fit	1	11	0.648	0.587	0.016	9.80	0.676	0.731
Spectral Type vs. SL Flux – initial fit	none	18	-0.541	-0.405	0.028	7.26	3.34	0.00
Spectral Type vs. SL Flux – final fit	1	17	-0.564	-0.485	0.010	6.19	3.12	0.00
Spectral Type vs. $\log(L_X/\text{erg s}^{-1})$	none	12	-0.464	-0.355	0.150	26.34	1.33	0.205
Spectral Type vs. $\log(\dot{M}_*/M_{\odot}yr^{-1})$	none	18	-0.269	-0.154	0.417	52.36	1.48	0.096
$\log(L_{\rm X}/{\rm erg~s^{-1}})$ vs. $\log(\dot{\rm M}_*/{\rm M_{\odot}yr^{-1}})$	none	12	-0.084	0.015	1.00	67.47	1.62	0.095

Note. — See description of parameters in Table 4 and in text.

^bPearson's r linear correlation coefficient, a measure of how closely two variables fit a linear relationship. |r| values closer to 1 indicate better correlation.

^cKendall's τ rank statistic, a measure of the degree of correlation between two parameters that does not assume normally distributed data. The closer $|\tau|$ is to 1, the better the correlation.

^d Two-sided P value, the probability (assuming no correlation) of obtaining a result at least as extreme as the result that is actually observed. The lower the P value, the higher the probability of correlation..

 $^{^{\}mathrm{e}}$ Probability of getting r from a random distribution of size n.

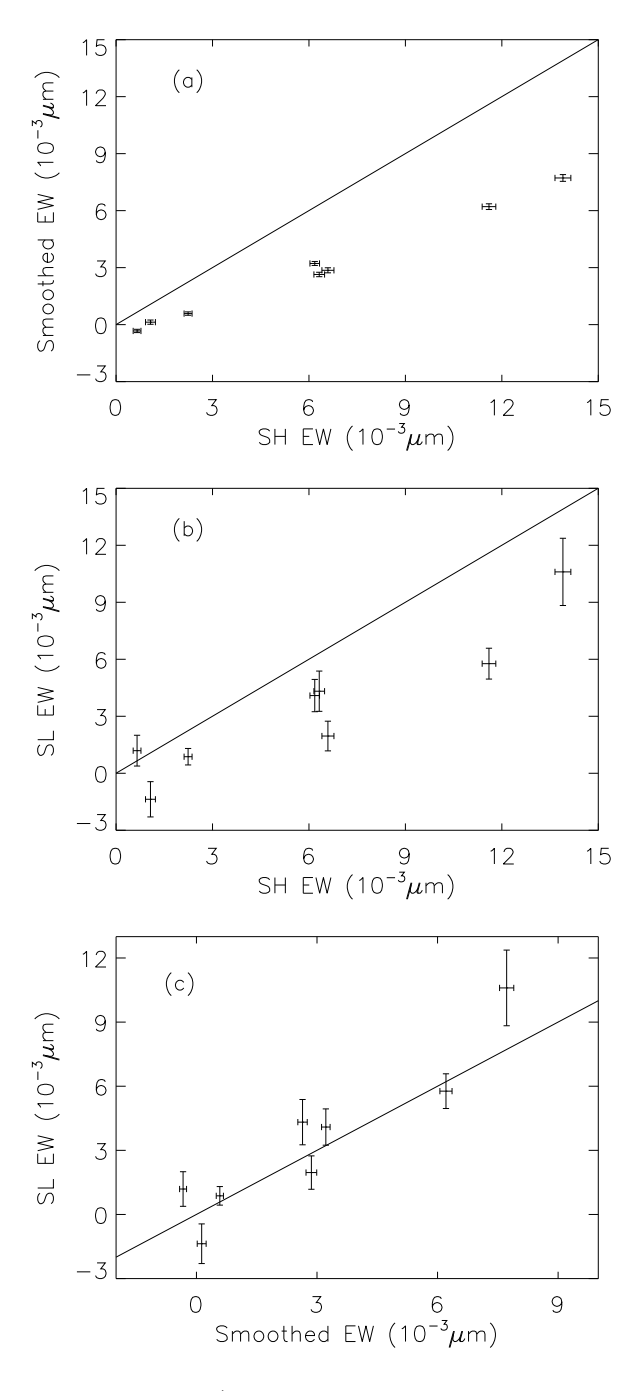


Fig. 3.— The comparison SH, smoothed/resampled and SL HCN equivalent widths (Tables 2 and 3). A unity line is shown for reference in each plot.

To summarize, while the SL measurements do not recover the HCN flux of the SH spectra, our results suggest that studies using SL spectra can recover quantitative trends in molecular emission

strength seen in higher resolution observations. The SL HCN measurements may therefore track the SH HCN measurements well enough to reveal interesting trends when compared with other T Tauri properties. We explore this possibility in the next section.

Although we refer to our SL measurements as "fluxes" and "equivalent widths", it is more useful to think of these quantities as *line* indices. The index can be positive (e.g., if there is HCN emission) or negative. The latter could occur either if there is either true absorption (e.g., as in IRS 46; Lahuis et al. 2006) or emission from other features in the "continuum" regions that are used to define the index.

In addition to the HCN emission feature, we also attempted a similar analysis for C_2H_2 ($\sim 13.7\,\mu\text{m}$) and an H_2O feature at $\sim 12.4\,\mu\text{m}$. We were unable to recover with the SL data emission strength trends seen in the SH data for these features, probably because they are weaker than HCN in spectra of T Tauri stars (Pascucci et al. 2009). We note that greater success may be possible with data analysis techniques more sophisticated than those used here. We also note that when we performed the same analysis using the Furlan et al. (2006) reduction of the SL data we did not find a significant correlation between SL and SH emission strengths, demonstrating that the specific data reduction procedure for the SL data can influence the ability to recover trends in SH data.

3.2. Variation in HCN Feature Strength

In our sample of SL spectra, the HCN flux varies from non-detections (below ~ 1 mJy- μ m) to over 5 mJy- μ m, and the HCN equivalent width varies over approximately an order of magnitude (see Table 2). What causes the strength of the HCN feature to differ in these systems? Although the sources have many similar properties (e.g., they have similar stellar masses and spectral types), the stellar accretion rate ($\dot{\rm M}_*$) and X-ray luminosity ($\rm L_X$) do vary across the sample, as may other physical properties not described here. To investigate whether stellar accretion rate and X-ray luminosity play a role in determining the HCN emission strength, we compared the HCN fluxes of the sources in the SL sample with their values of $\dot{\rm M}_*$ and $\rm L_X$ from the literature (Table 1).

In Figure 4, panels (a), (b), and (c) plot SL HCN flux against stellar accretion rate, stellar X-ray luminosity, and spectra type, respectively. Panels (d), (e), and (f) plot these three quantities – accretion rate, X-ray luminosity, and spectral type – against each other. The distribution of points suggests possible trends between SL HCN flux and the quantities in Fig. 4a, b, c, although these trends, if they exist, are not extremely tight. The lack of a tight correlation is perhaps not surprising since many physical and chemical processes (e.g., heating that is unrelated to accretion, chemical synthesis, photodestruction, excitation conditions) can potentially affect the strength of any given molecular emission feature. As a result, outliers in any trend are to be expected, e.g., if some systems have managed to synthesize more or less HCN. We therefore employed the following simple rejection scheme when examining our data for possible trends: we performed a weighted linear fit, including uncertainties in both the x- and y-directions, to all of the data in Fig. 4a, b, and

c and iteratively rejected the top one to two outliers, all of which were above 3.3- σ . The outliers are plotted as open triangles in Fig. 4, and a summary of the fit statistics is given in Table 5. Table 5 also reports the reduced χ^2 of the linear fit and q, the probability that a correct model would give a χ^2 value equal to or larger than the observed χ^2 .

In the case of Fig. 4a, where we plot SL HCN flux versus stellar accretion rate, the Pearson's r-value associated with all of the data points shown is 0.53 and the $\tau_{Kendall}$ value is 0.39 (see Table 5). Rejection of the top two outliers at 3.6 σ and 3.8 σ (open symbols) resulted in a Pearson's r-value associated with the remaining data points of 0.66 and the $\tau_{Kendall}$ value of 0.57 (see also Table 5), suggesting a potential positive correlation between stellar accretion rate and HCN flux.

Even with outlier rejection, there is still significant scatter, which is perhaps to be expected, as discussed above. In addition, the difficulty in determining precise veiling and bolometric corrections likely introduces systematic uncertainty in stellar accretion rate measurements, as discussed by Hartigan et al. (1991) and Gullbring et al. (1998). These authors also note that time variability, as a result of intrinsic fluctuation in the accretion rate or the modulation of a nonaxisymmetric magnetosphere, can contribute to the uncertainty; they suggest a cumulative uncertainty of ~ 3 in stellar accretion rate (Hartigan et al. 1991; Gullbring et al. 1998). We represent this uncertainty by the horizontal bar in the lower left corner of Fig. 4a.

For Fig. 4b, which shows SL HCN flux versus stellar X-ray luminosity, the associated Pearson's r-value for all of the data points is 0.40 and the $\tau_{Kendall}$ value is 0.38 (see Table 5). Rejection of the top outlier at 3.3 σ (open symbol) resulted in a Pearson's r-value associated with the remaining data points of 0.65 and the $\tau_{Kendall}$ value of 0.59 (see also Table 5), suggesting a potential positive correlation between stellar X-ray luminosity and HCN flux. The larger p_{rand} and P_{τ} for these data (compared to those shown in Fig. 4a or 4c; see Table 5) are partly a result of the smaller sample size n (12 versus 18 objects). Some of the scatter in this plot is likely the result of variability in L_X . Güdel et al. 2010 notes that the range of uncertainty in X-ray flux determination is dominated by variability on various time scales, and (apart from singular flares) is typically characterized by flux variations within a factor of two from low to high levels. We represent this uncertainty by the horizontal error bar in the lower left corner Fig. 4b.

Fig. 4c shows SL HCN flux versus stellar spectral type. The associated Pearson's r-value for all of the data points is -0.54 and the $\tau_{Kendall}$ value is -0.41 (see Table 5). Rejection of the top outlier $3.5\,\sigma$ (open symbol) resulted in a Pearson's r-value associated with the remaining data points of -0.56 and the $\tau_{Kendall}$ value of -0.49 (see also Table 5). An estimated spectral type error of 0.5 subclass is much smaller than the dispersion of the points. While the statistics suggest a possible negative correlation between spectral type and HCN flux, it seems unlikely that spectral type (and therefore stellar temperature) directly affects the HCN flux from the disk; while the HCN flux in our sample varies over almost an order of magnitude, the range of spectral types we studied is relatively narrow, spanning $\sim 1400\,\mathrm{K}$ in temperature.

Fig. 4d may shed some light on this issue. It shows that within our sample, X-ray luminosity

decreases on average with later spectral type. The associated Pearson's r-value for all the objects plotted is -0.46, and the $\tau_{Kendall}$ value is -0.36 (see Table 5). This modest correlation in our sample is also supported by larger samples of pre-main sequence stars (e.g., Winston et al. 2010; Preibisch et al. 2005); our examination of those data show a similar decrease in X-ray luminosity with later spectral type. This trend between X-ray luminosity and spectral type could be explained as a consequence of the rough proportionality between L_X and L_* in pre-main sequence stars, with $L_X/L_* \sim 10^{-4} - 10^{-3}$ (Telleschi et al. 2007; Preibisch et al. 2005). Among stars in Myr-old populations such as those in our sample, L_* also decreases with later spectral type (Stelzer & Neuhäuser 2001; Preibisch et al. 2005; Winston et al. 2010), so L_X would also be expected to decrease with later spectral type in our sample. Thus, the trend in Fig. 4c may not reflect a fundamental relationship between HCN flux and spectral type, but instead results from the two underlying relations between L_X and HCN flux (Fig. 4b) and L_X decreasing with later spectral type (Fig. 4d).

Another possibility is that the luminosity associated with accretion (L_{acc}) is decreasing with later spectral type and this is what drives the trend of HCN flux with spectral type. The average accretion rate is known to decrease with decreasing mass (later spectral type), but the spread at any given mass is \sim two orders of magnitude (Muzerolle et al. 2005). In Fig. 4e, we plot stellar accretion rate versus spectral type. There is no strong correlation (see Table 5) within the narrow range of spectral type of our sample, consistent with Muzerolle et al. (2005). In Fig. 4f, we plot the stellar X-ray luminosity versus the stellar accretion rate. The comparison also shows no correlation (see Table 5).

Because our data set is small (and our analysis methods explorative), larger samples of IRS spectra are needed to confirm that any trends exist and test whether any of the fits proposed are reasonable representations of the trend. Our sample is artificially sparse at high accretion rates due to the difficulty in measuring HCN emission from low resolution spectra of high-accretion sources; their enhanced continuum flux reduces the contrast of emission features above the continuum. Thus it would be useful to expand the sample to include more sources covering the same range of stellar accretion rates as well as a larger range of accretion rates. If HCN flux and stellar accretion rate are correlated, we would expect that sources with accretion rates $< 10^{-9} \,\mathrm{M_{\odot}yr^{-1}}$ would have low to undetectable HCN fluxes. Similarly, we would expect that sources with X-ray luminosities below $\sim 6.3 \times 10^{28} \,\mathrm{erg \ s^{-1}}$ would not show detectable HCN, and that sources with X-ray luminosities above $\sim 2.5 \times 10^{30} \,\mathrm{erg \ s^{-1}}$ might continue to show enhanced HCN emission with increasing X-ray flux.

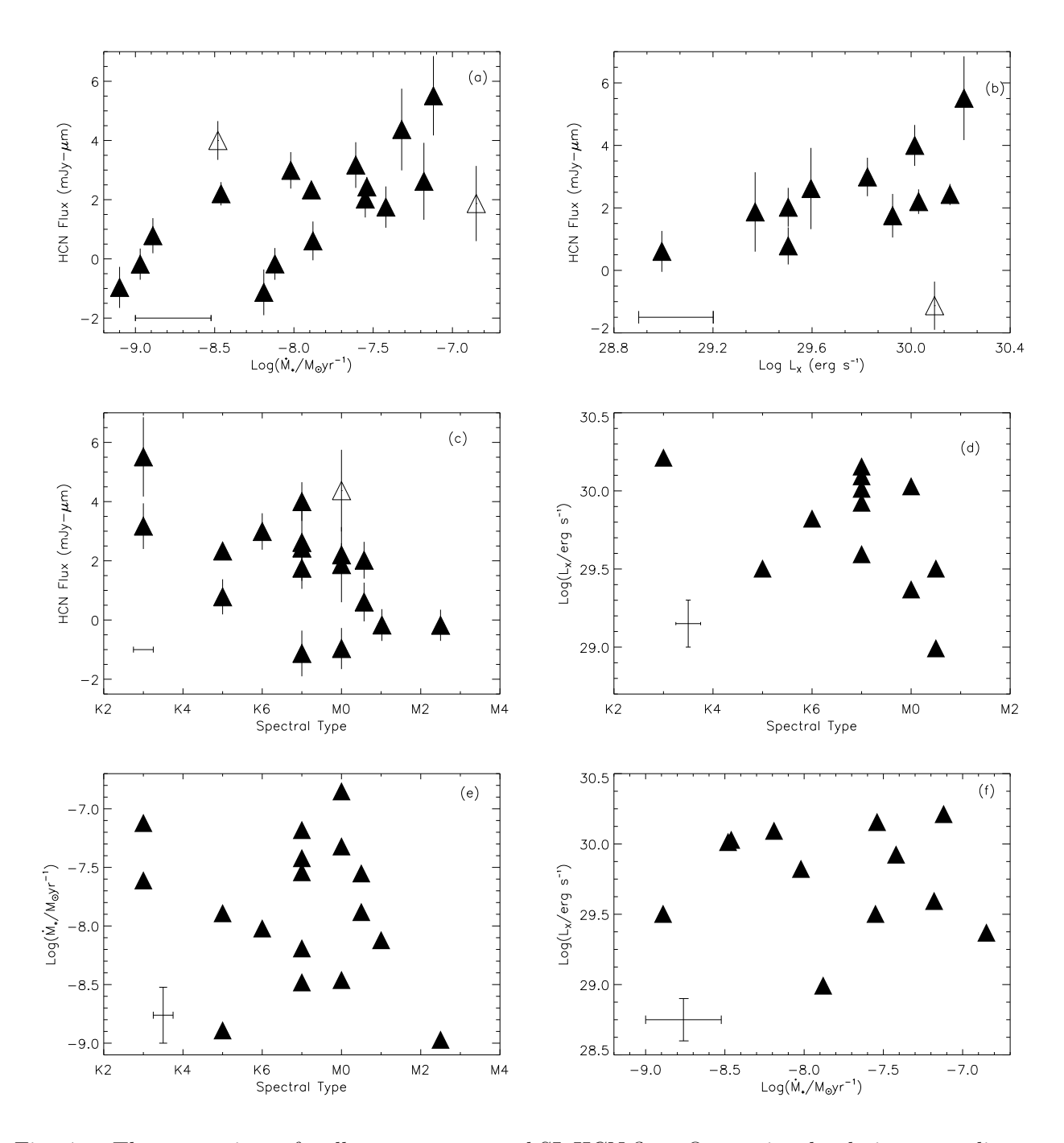


Fig. 4.— The comparison of stellar parameters and SL HCN flux. Open triangles designate outliers identified by iterative rejection. (a) SL HCN flux versus stellar accretion rate ($\dot{\rm M}_*$). (b) SL HCN flux versus stellar X-ray luminosity ($\rm L_X$). (c) SL HCN flux versus spectral type. (d) $\rm L_X$ versus spectral type. (e) $\dot{\rm M}_*$ versus spectral type. (f) $\rm L_X$ versus $\dot{\rm M}_*$.

4. Discussion

We find that SH and SL measurements of the 14 μ m HCN feature are correlated in our small sample of T Tauri stars. Our results support the work of Pascucci et al. (2009), who used these SL spectra as part of their larger sample to deduce the differences between gaseous disks surrounding T Tauri stars and those surrounding lower mass stars and brown dwarfs. That study showed a prominent difference in the relative detection rates of HCN and C_2H_2 between the two samples, with HCN detected more commonly in TTS than in the lower mass objects. The median spectra they created of samples of T Tauri stars and the lower mass objects showed that the flux ratio of HCN to C_2H_2 is ~ 3 for T Tauri stars and much lower, ~ 0.2 , for the lower mass objects. Our results show that such comparisons can be extended to comparisons of HCN feature fluxes in the spectra of individual objects.

We also find potential trends between the SL HCN flux index and stellar accretion rate, X-ray luminosity, and stellar spectral type. With respect to the potential trend with stellar accretion rate, a similar relation between CO fundamental emission and stellar accretion rate has been reported in TTS and Herbig Ae-Be stars (Najita et al. 2003; Brittain et al. 2007). These authors suggest that a correlation between CO emission and accretion rate would be expected if accretion-related processes heat the disk atmosphere. In a related study of transition objects, Salyk et al. (2009) report that the sources in their sample that show inner-disk CO fundamental emission have higher accretion rates. The sources that display CO fundamental emission also display $Pf\beta$ emission, which is moderately correlated with the accretion diagnostic $H\alpha$. Accretion-related processes could strengthen the HCN emission by enhancing the temperature, and/or the HCN abundance, in the disk atmosphere.

The effect of accretion-related heating on disk molecular emission has been studied by Glassgold et al. (2004, 2009). They proposed two sources of mechanical heating in the disk atmosphere: viscous accretion, possibly generated by the magnetorotational instability (MRI; Stone et al. 2000), and stellar wind interaction with the disk surface (Glassgold et al. 2004). Glassgold et al. (2009) invoked mechanical heating, due to one or both of these sources, in addition to the formation of $\rm H_2$ on warm grains, to explain the large column densities of warm $\rm H_2O$ that are observed in emission in disk atmospheres. Glassgold et al. (2009) determined that these processes can increase the thickness of the warm water column to the extent reported by Carr & Najita (2008) and Salyk et al. (2008). If mechanical heating does affect the thermal-chemical structure of disk atmospheres in this way, and if higher accretion rates and higher rates of mechanical heating derive from the same physical mechanism, we would expect to see a correlation between accretion rate and $\rm H_2O$ feature strength. Accretion rate may play a similar role in enhancing HCN emission strength, i.e. by increasing the column density of warm HCN in the disk atmosphere.

There may be an additional chemical connection between H₂O and HCN emission, with efficient water formation possibly leading to an enhanced HCN abundance. As described by Lahuis & van Dishoeck (2000), efficient H₂O formation will drive most of the available oxygen into H₂O, resulting

in a lower abundance of gaseous O₂. Since O₂ would otherwise react with atomic carbon, the lack of O₂ could lead to an enhanced atomic C abundance and in turn a larger HCN abundance (e.g., via the reaction scheme described by Agundez et al. 2008). Perhaps for this reason, hot cores that are found to have the highest gas phase H₂O abundances are also those with the highest HCN abundances (e.g., van Dishoeck 1998; Lahuis & van Dishoeck 2000). Thus accretion-related mechanical heating in disks may enhance disk HCN emission both thermally, by producing a deeper temperature inversion at the disk surface, and chemically, by enhancing the HCN abundance as a consequence of efficient water formation. Detailed modeling is needed to explore these possibilities.

Increased UV irradiation produced by higher stellar accretion may also enhance the HCN abundance. Using Agúndez et al. (2008) as a guide, Pascucci et al. (2009) argued that the HCN abundance in disk atmospheres may be limited by the availability of atomic nitrogen and that the atomic nitrogen abundance depends primarily on the dissociation of N_2 via UV-dissociation. Thus, HCN would be brighter for sources with more energetic UV flux (i.e., higher accretion rate), while C_2H_2 (not requiring nitrogen to form) would not vary. This may explain their finding that T Tauri stars have stronger HCN emission relative to C_2H_2 than lower mass stars and brown dwarfs, as these lower mass objects would have lower photospheric UV emission and lower accretion rates than TTS. The range in stellar accretion rate among T Tauri stars may induce a range in their HCN abundances for similar reasons.

Another factor that may play a role in setting the HCN flux from the disk is X-ray irradiation, based on Fig. 4b. The effect of X-ray irradiation on the thermal-chemical structure of disks has been investigated previously by Glassgold et al. (2004, 2009), although they did not specifically study HCN. X-ray irradiation may enhance the abundance of molecular ions and radicals that lead to enhanced HCN emission. Further modeling is needed to investigate the relative roles of X-ray and UV irradiation in this context.

We find a possible trend of HCN flux decreasing with stellar spectral type (Fig. 4c). While this is in the spirit of the trend found by Pascucci et al. (2009), it is unlikely that stellar spectral type itself (i.e., stellar temperature) is affecting the HCN flux for this small sample of TTS. The other two processes we examined, stellar accretion rate and stellar X-ray flux (and/or other processes not yet identified) are likely to have a more direct influence on the HCN flux. Stellar accretion rate is not well correlated with spectral type (see Fig. 4e) and the TTS in our sample span a small mass range, so the resulting accretion luminosity seems unlikely to be correlated over the range of spectral types that we studied. In comparison, L_X shows a possible correlation with spectral type (Fig. 4d), so it may be responsible for the moderate correlation of HCN flux with spectral type.

Several of the objects in our sample (plotted as open triangles in Fig. 4a, b, and c) appear to deviate from the possible trends we identify here. The dispersion we observe could arise from differences in disk structure (e.g., flaring) and composition that may originate from the natal environment as well as the dynamic processing that occurs within the disk lifetime. This makes the objects that deviate from our observed trends not only expected, but of particular interest. For

example, while variations in stellar accretion rate are typically factors of ~ 2 or less (Hartigan et al. 1991), stellar accretion rates of some individual sources may vary up to an order of magnitude on timescales of ~ 1 yr (Alencar & Batalha 2002). This could induce a significant shift for some objects in our plots. Variability in the stellar accretion rate could also affect the time-averaged disk chemistry. Similar considerations might apply for stellar X-ray variability.

Another potential cause of dispersion is a different or additional heating source. The strength of the UV irradiation striking the disk may depend on the absorption along the line-of-sight, e.g., in a magnetosphere or an intervening wind (e.g., Alexander et al. 2004; Ercolano et al. 2008, 2009; Gorti & Hollenbach 2008, 2009). This could influence the temperature and chemical processing of the disk atmosphere, as might radial transport or vertical mixing between the upper layer and regions closer to the disk midplane (e.g., Bergin et al. 2007; Turner et al. 2006; Semenov et al. 2006; Willacy et al. 2006).

Dust sedimentation can also increase the line-to-continuum contrast of molecular emission (Glassgold et al. 2004; Dullemond et al. 2007), and such emission is more commonly detected in more highly settled disks (Salyk et al. 2011). The properties and distribution of grains are known to vary widely over disk age and structure (e.g., Watson et al. 2009). If molecular formation (e.g., H₂) on grains influences disk chemical synthesis, variations in grain properties may lead to variations in observable molecular features (Glassgold et al. 2009). In the panels of Figure 4, there are several outlying points whose HCN flux index is enhanced or depleted relative to the rest of the points. These might be ideal systems in which to look for additional chemical peculiarity or heating mechanisms that could be affecting the molecular emission strength.

The trends described here require a larger sample to confirm. In tandem, it may be possible to expand the wavelength range we analyze by considering observations from Spitzer IRS modules that cover a wider wavelength range (i.e., Long-High, $20\,\mu\mathrm{m}-40\,\mu\mathrm{m}$) and more molecular species. Additional high resolution data would also help verify the technique of using SL spectra to recover real trends.

5. Summary & Conclusions

Our goal was to investigate the extent to which lower resolution Spitzer IRS data can be used to recover quantitative molecular emission trends seen in higher resolution Spitzer IRS data. We have shown that a simple prescription for measuring the strength of the 14 μ m HCN emission feature, when applied to low resolution Spitzer data, can recover trends in HCN emission strength that are seen in high resolution Spitzer data. Additionally, we report possible correlations between HCN flux and stellar accretion rate, and HCN flux and stellar X-ray luminosity, that may originate from accretion-driven mechanical heating and/or photochemistry at work in the inner disk atmosphere. While qualitative comparisons of the presence of line emission were possible and successful earlier (e.g., Pascucci et al. 2009), our results demonstrate that quantitative comparisons of the line

intensities can also be carried out.

What controls the presence and strength of organic molecular features such as HCN in the planet-forming regions around young stars? One challenge in addressing this question is the large number of physical and chemical processes that can potentially affect the molecular emission strength, as discussed in §4. Our methods and results show that the large number of low resolution disk spectra that reside in the *Spitzer* archive could be used in future demographic studies to attempt to identify the relevant processes.

Facilities: Spitzer ()

REFERENCES

- Agúndez, M., Cernicharo, J., & Goicoechea, J. R. 2008, A&A, 483, 831
- Alencar, S. H. P., & Batalha, C. 2002, ApJ, 571, 378
- Alexander, R. D., Clarke, C. J., & Pringle, J. E. 2004, MNRAS, 354, 71
- Apai, D., & Lauretta, D. S. 2010, Protoplanetary Dust: Astrophysical and Cosmochemical Perspectives, 128
- Ardila, D. R., & Basri, G. 2000, ApJ, 539, 834
- Bergin, E. A., Aikawa, Y., Blake, G. A., & van Dishoeck, E. F. 2007, Protostars and Planets V, 751
- Bergin, E., et al. 2004, ApJ, 614, L133
- Berthoud, M. G., Keller, L. D., Herter, T. L., Richter, M. J., & Whelan, D. G. 2007, ApJ, 660, 461
- Blake, G. A., & Boogert, A. C. A. 2004, ApJ, 606, L73
- Blum, R. D., Barbosa, C. L., Damineli, A., Conti, P. S., & Ridgway, S. 2004, ApJ, 617, 1167
- Brittain, S. D., Simon, T., Najita, J. R., & Rettig, T. W. 2007, ApJ, 659, 685
- Carmona, A. 2010, Earth Moon and Planets, 106, 71
- Carr, J.S., & Najita, J.R. 2011, ApJ, submitted
- Carr, J.S., & Najita, J.R. 2008, Science, 319, 1504
- Carr, J. 2005, High Resolution Infrared Spectroscopy in Astronomy, 203
- Carr, J. S., Tokunaga, A. T., & Najita, J. 2004, ApJ, 603, 213
- Carr, J. S., Mathieu, R. D., & Najita, J. R. 2001, ApJ, 551, 454
- Carr, J. S., Tokunaga, A. T., Najita, J., Shu, F. H., & Glassgold, A. E. 1993, ApJ, 411, L37
- Chandler, C. J., Carlstrom, J. E., Scoville, N. Z., Dent, W. R. F., & Geballe, T. R. 1993, ApJ, 412, L71
- Dullemond, C. P., Hollenbach, D., Kamp, I., & D'Alessio, P. 2007, Protostars and Planets V, 555
- Dutrey, A., Guilloteau, S., & Ho, P. 2007, Protostars and Planets V, 495
- Dutrey, A., Guilloteau, S., Prato, L., Simon, M., Duvert, G., Schuster, K., & Menard, F. 1998, A&A, 338, L63

Dutrey, A., Guilloteau, S., Duvert, G., Prato, L., Simon, M., Schuster, K., & Menard, F. 1996, A&A, 309, 493

Ercolano, B., Clarke, C. J., & Drake, J. J. 2009, ApJ, 699, 1639

Ercolano, B., Drake, J. J., Raymond, J. C., & Clarke, C. C. 2008, ApJ, 688, 398

Furlan, E., et al. 2006, ApJS, 165, 568

Glassgold, A. E., Meijerink, R., & Najita, J. R. 2009, ApJ, 701, 142

Glassgold, A. E., Najita, J., & Igea, J. 2004, ApJ, 615, 972

Gorti, U., & Hollenbach, D. 2009, ApJ, 690, 1539

Gorti, U., & Hollenbach, D. 2008, ApJ, 683, 287

Güdel, M., et al. 2010, A&A, 519, A113

Guilloteau, S., & Dutrey, A. 1998, A&A, 339, 467

Gullbring, E., Hartmann, L., Briceno, C., & Calvet, N. 1998, ApJ, 492, 323

Hartigan, P., Strom, K. M., & Strom, S. E. 1994, ApJ, 427, 961

Hartigan, P., Kenyon, S. J., Hartmann, L., Strom, S. E., Edwards, S., Welty, A. D., & Stauffer, J. 1991, ApJ, 382, 617

Hartmann, L., Calvet, N., Gullbring, E., & D'Alessio, P. 1998, ApJ, 495, 385

Henning, T., & Meeus, G. 2009, arXiv:0911.1010

Herczeg, G. J., Linsky, J. L., Walter, F. M., Gahm, G. F., & Johns-Krull, C. M. 2006, ApJS, 165, 256

Herczeg, G. J., Linsky, J. L., Valenti, J. A., Johns-Krull, C. M., & Wood, B. E. 2002, ApJ, 572, 310

Houck, J. R., et al. 2004, ApJS, 154, 18

Kastner, J. H., Zuckerman, B., Weintraub, D. A., & Forveille, T. 1997, Science, 277, 67

Kenyon, S.J., & Hartmann, L. 1995, ApJS, 101, 117

Lahuis, F., et al. 2006, ApJ, 636, L145

Lahuis, F., & van Dishoeck, E. F. 2000, A&A, 355, 699

Millan-Gabet, R., Malbet, F., Akeson, R., Leinert, C., Monnier, J., & Waters, R. 2007, Protostars and Planets V, 539

- Muzerolle, J., Luhman, K. L., Briceño, C., Hartmann, L., & Calvet, N. 2005, ApJ, 625, 906
- Najita, J. R., Doppmann, G. W., Carr, J. S., Graham, J. R., & Eisner, J. A. 2009, ApJ, 691, 738
- Najita, J. R., Crockett, N., & Carr, J. S. 2008, ApJ, 687, 1168
- Najita, J. R., Carr, J. S., Glassgold, A. E., & Valenti, J. A. 2007a, Protostars and Planets V, 507
- Najita, J. R., Strom, S. E., & Muzerolle, J. 2007b, MNRAS, 378, 369
- Najita, J., Carr, J. S., & Mathieu, R. D. 2003, ApJ, 589, 931
- Najita, J. R., Edwards, S., Basri, G., & Carr, J. 2000, Protostars and Planets IV, 457
- Najita, J., Carr, J. S., Glassgold, A. E., Shu, F. H., & Tokunaga, A. T. 1996, ApJ, 462, 919
- Natta, A., Testi, L., Calvet, N., Henning, T., Waters, R., & Wilner, D. 2007, Protostars and Planets V, 767
- Pascucci, I., Apai, D., Luhman, K., Henning, T., Bouwman, J., Meyer, M. R., Lahuis, F., & Natta, A. 2009, ApJ, 696, 143
- Preibisch, T., et al. 2005, ApJS, 160, 401
- Pontoppidan, K. M., Salyk, C., Blake, G. A., Meijerink, R., Carr, J. S., & Najita, J. 2010, arXiv:1006.4189
- Pontoppidan, K. M., Blake, G. A., van Dishoeck, E. F., Smette, A., Ireland, M. J., & Brown, J. 2008, ApJ, 684, 1323
- Qi, C., Wilner, D. J., Aikawa, Y., Blake, G. A., & Hogerheijde, M. R. 2008, ApJ, 681, 1396
- Salyk, C., Pontoppidan, K. M., Blake, G. A., Najita, J., & Carr, J. 2011, ApJ, accepted
- Salyk, C., Blake, G. A., Boogert, A. C. A., & Brown, J. M. 2009, ApJ, 699, 330
- Salyk, C., Pontoppidan, K. M., Blake, G. A., Lahuis, F., van Dishoeck, E. F., & Evans, N. J., II 2008, ApJ, 676, L49
- Salyk, C., Blake, G. A., Boogert, A. C. A., & Brown, J. M. 2007, ApJ, 655, L105
- Semenov, D., Wiebe, D., & Henning, T. 2006, ApJ, 647, L57
- Semenov, D., Pavlyuchenkov, Y., Schreyer, K., Henning, T., Dullemond, C., & Bacmann, A. 2005, ApJ, 621, 853
- Stelzer, B., & Neuhäuser, R. 2001, A&A, 377, 538
- Stone, J. M., Gammie, C. F., Balbus, S. A., & Hawley, J. F. 2000, Protostars and Planets IV, 589

Telleschi, A., Güdel, M., Briggs, K. R., Audard, M., & Palla, F. 2007, A&A, 468, 425

Thi, W.-F., & Bik, A. 2005, A&A, 438, 557

Thi, W.-F., van Dalen, B., Bik, A., & Waters, L. B. F. M. 2005, A&A, 430, L61

Thi, W.-F., van Zadelhoff, G.-J., & van Dishoeck, E. F. 2004, A&A, 425, 955

Turner, N. J., Willacy, K., Bryden, G., & Yorke, H. W. 2006, ApJ, 639, 1218

Valenti, J. A., Johns-Krull, C. M., & Linsky, J. L. 2000, ApJS, 129, 399

van Dishoeck, E. F. 1998, The Molecular Astrophysics of Stars and Galaxies, edited by Thomas W. Hartquist and David A. Williams. Clarendon Press, Oxford, 1998., p.53, 4, 53

Watson, D. M., et al. 2009, ApJS, 180, 84

Willacy, K., Langer, W., Allen, M., & Bryden, G. 2006, ApJ, 644, 1202

Winston, E., et al. 2010, AJ, 140, 266

This preprint was prepared with the AAS LATEX macros v5.2.